

# MOF-derived Porous NiO Nanorod and Microflower Structures with Enhanced Non-enzymatic Glucose Electrochemical Sensing Performance

Xiaobei Zhang<sup>1</sup>, Rui Wang<sup>2</sup>, Yaqing Wei<sup>2</sup>, Xiaoqi Pei<sup>2</sup>, Zhuo Zhou<sup>2</sup>, Jingchao Zhang<sup>2</sup>,  
Renchun Zhang<sup>2</sup>, Daojun Zhang<sup>2,\*</sup>

<sup>1</sup> College of Chemistry, Zhengzhou University, 100 Science Road, Zhengzhou 450001, P. R. China

<sup>2</sup> Henan Key Laboratory of New Optoelectronic Functional Materials, College of Chemistry and Chemical Engineering, Anyang Normal University, Anyang 455000, Henan, China

\*E-mail: [zhangdj0410@sohu.com](mailto:zhangdj0410@sohu.com), [zjc19830618@126.com](mailto:zjc19830618@126.com)

Received: 5 December 2020 / Accepted: 8 February 2021 / Published: 28 February 2021

---

The porous and hierarchical structure with plentiful electroactive sites may ensure high activity and stability in electrocatalytic oxidation glucose by accelerating the transport of analyzer and electron during the electrochemical process. Thus, to design and fabricate electrode materials with different structures and morphology is still an appreciation method to promote electrochemical performance. In this work, two morphology of porous NiO structures were synthesized by the MOF-derived precursors after the calcination process. The obtained NiO structures prepared by thermal conversion of Ni-BTEC and Ni-PTA frameworks at mild temperature conditions not only possess the nanorods and microflowers morphology of the MOF precursors but also exhibit large surface area, which could be used as the enzyme-free catalyst for glucose electrooxidation in the basic supporting electrolyte. The result indicates that MOF-derived porous NiO nanorods and microflowers may be potential electrode materials for glucose electrochemical sensing.

---

**Keywords:** porous NiO structure; nanorods; microflowers; enzyme-free glucose sensor; electrocatalysts

## 1. INTRODUCTION

In recent years, electrochemical sensors based on transition metal compounds has received widespread interest due to their low cost and easy preparation [1-3]. Using abundant elements on earth instead of noble metal to fabricate electrode materials is appreciated. To date, a great deal of transition metal oxides (TMOs) such as NiO [4, 5], CuO [6,7], Co<sub>3</sub>O<sub>4</sub> [8, 9], CuCo<sub>2</sub>O<sub>4</sub> [10], and NiCo<sub>2</sub>O<sub>4</sub> [11,12] micro/nanostructures have been investigated as electrode materials for electrochemical sensing. Many factors of modified electrode materials include surface morphology, microstructure and composition can

affect the electrochemical sensing performances. Porous micro/nanostructures have attracted great attention in nonenzymatic electrochemical sensing consist of glucose, hydrogen peroxide, hydrazine, glutathione, dopamine, and etc.

The glucose level in the blood can reflect and management of the diabetes signal of the people, thus the fast and accurate detection of glucose concentration is an important research topic [13]. In recent years, the non-enzymatic electrochemical glucose sensor based on TMOs have been recognized as the preferable candidate due to their inherent stability and good performance. Fabricating micro/nanostructures with controllable morphology is available to tune the specific surface area of the electrode materials, which will facilitate the glucose electro-oxidation kinetics. In recent years, porous micro/nano-materials achieved from the transformation of metal-organic frameworks (MOFs) precursors usually exhibited excellent performance in electrocatalysts, supercapacitors, and chemical sensors [14,15]. The micro/nano-structure derived from MOFs provides a large surface area and connected porous architecture for the charge transfer and the diffusion of electrolyte and analyte within the electrode, which facilitate the kinetic-controlled electrochemical glucose oxidation processes. Nickel oxides are more stable in an alkaline environment than sulfides, however, the common nickel oxides nano-catalysts are easy to aggregate on the surface of the electrode, leading to weakening electrochemical performance. NiO structures derived from MOFs can keep the skeleton of parent precursors without agglomeration, providing abundant surface area and inner space for glucose detection and electron transport [16,17]. Furthermore, the design and synthesis of NiO nanostructure avoid the use of additional template, such as Cu<sub>2</sub>O nanospheres [18] and carbon microspheres [19], thus the obtain morphology of NiO is rich and more variable. Taking into account the above reasons, in this work, we utilize a self-sacrificial template strategy based on direct annealing Ni-MOF precursors at middle temperature to prepare porous NiO nanorods and microflowers, the as-obtained porous NiO structures preserve the original Ni-MOF morphology well. Further research manifests that NiO nanorods and microflowers modified glass carbon electrodes exhibit superior performance in detecting glucose and may act as potential enzyme-free glucose sensors in the future.

## 2. EXPERIMENTAL SECTION

### 2.1 Synthesis of NiO porous nanorods

First, nickel (II) 2,4-pentanedionate (0.5g, 1.95 mmol) and pyromellitic acid (H<sub>4</sub>btec) (0.5g, 1.97 mmol) were dispersed in 5.0 mL of N-N-dimethylformamide (DMF), 5.0 mL of ethanol, and 5.0 mL of H<sub>2</sub>O with vigorous stirring for about 20 min, then heated at 160 °C in oven for 12 h. The obtained green powder was isolated via centrifugation and washed by ethanol/H<sub>2</sub>O (v/v=1:1) three times, then heated to 400 °C in muffle furnace at a heating rate of 2 °C min<sup>-1</sup> and kept for 2 h under atmosphere.

### 2.2 Synthesis of NiO porous microflowers

Nickel nitrate hexahydrate (0.0291g, 0.1 mmol) and p-phthalic acid (PTA) (0.0166g, 0.1 mmol) were dissolved in the mixture solution of N-N-dimethylacetamide (DMA, 3.6 mL) and alcohol (2.4 mL)

under continues stirring at room temperature for 30 min, and then kept in 140 °C for 4 h. The obtained sample (Ni-PTA MOF) were centrifuged by ethanol and deionized water (v/v=1:1), and dried at 60 °C. The NiO microflowers was prepared by the same sintering process as above mentioned.

### 2.3 Preparation and measurement of glucose sensor electrodes

1.0 mg of the above two kinds of NiO catalysts was dispersed to 1.0 mL ultrapure water under sonication, respectively. After that, 5.0  $\mu\text{L}$  of the catalyst inks were dropped on burnished GC electrode (3 mm) and dried at room temperature naturally. The electrochemical glucose detection was researched in a three-electrode setup by using Ag/AgCl as the reference electrode, platinum wire as the counter electrode, and NiO modified GC electrode as the working electrode. All the electrochemical experiments were conducted at room temperature under mild stirring.

## 3. RESULTS AND DISCUSSION

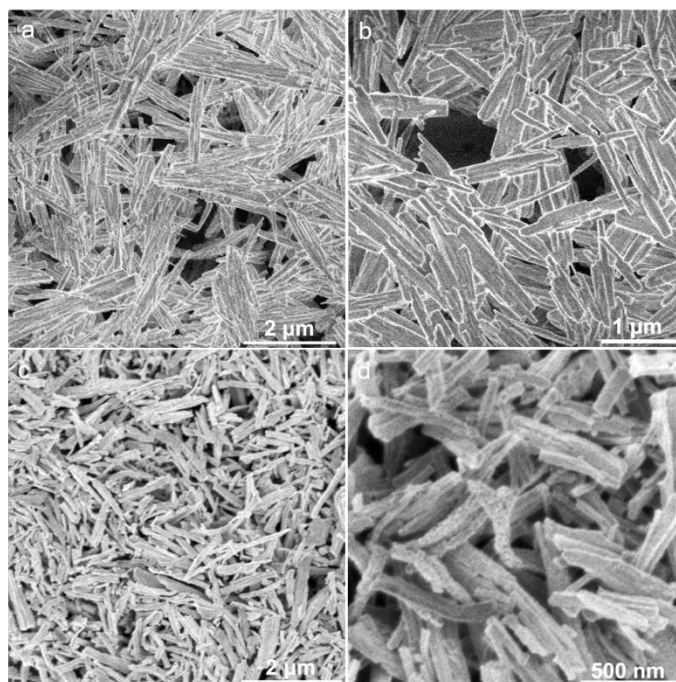


**Figure 1.** (a-b) The FESEM images of the Ni-BTEC MOF precursors, (c-d) the NiO nanorods derived from Ni-BTEC MOF after calcination.

The SEM images of the as-prepared Ni-BTEC MOF precursors before and after calcination are shown in Fig.1. The Ni-BTEC MOF nanorods are smooth and well-distributed, the morphology can be retained after calcination but the surface seems rough and porous. Through statistics of one hundred particles, the average size of the Ni-BTEC MOF-derived NiO nanorods is approximately 500 nm in length and 100 nm in width. The derived NiO nanorods maintain the initial precursor morphology well with dimension shrinkage, however, after calcination, the obtained particles exhibited enriched porous architecture, which was observed in TEM images (Fig.2a-c), suggests potential good properties. The

HRTEM image of the NiO nanorod indicates the presence of clear lattice fringes, and the lattice interplanar space of 0.245 nm corresponds to the (111) crystal plane of NiO (Fig.2d).

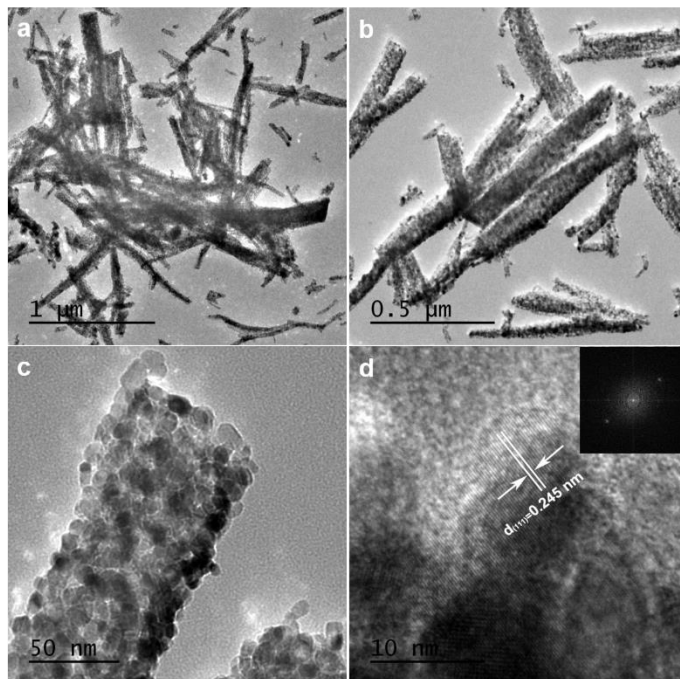


**Figure 2.** (a-b) TEM images of the NiO nanorods derived from Ni-BTEC MOF, (c-d) HRTEM image of NiO nanorods.

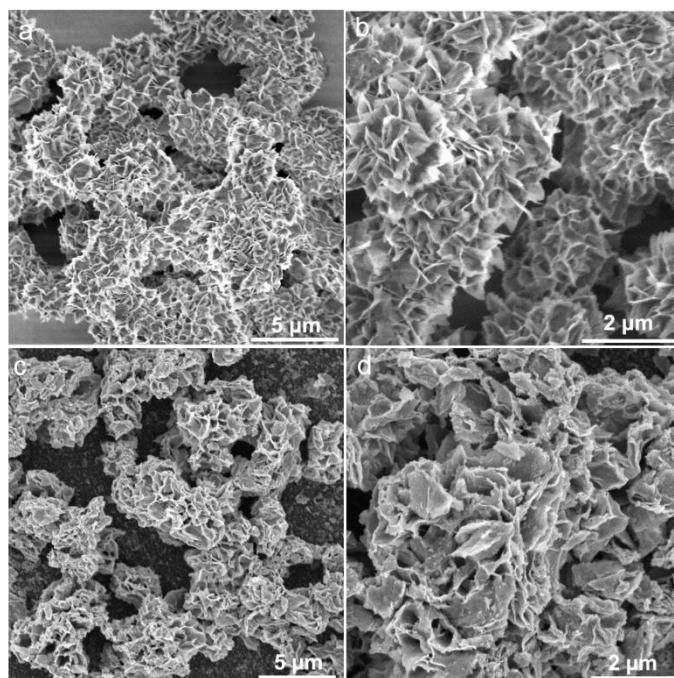


**Figure 3.** (a-b) SEM images of Ni-PTA MOF precursors, (c-d) The NiO microflowers obtained from the annealed Ni-PTA MOF.

As shown in Fig.3a-b, the Ni-PTA MOF microflowers was assembled by numberless ultrathin

nanosheets, the morphology can be retained after calcination, but the aggregation degree of nanosheets increase and become fragile (Fig.3c-d). In the TEM image shown in Fig.4a-c, the NiO microflowers contains numbers of nanoparticles, the lattice spacing of the NiO microflowers corresponds to the (111) plane of NiO (Fig.4d), indicating the calcined product was pure NiO.

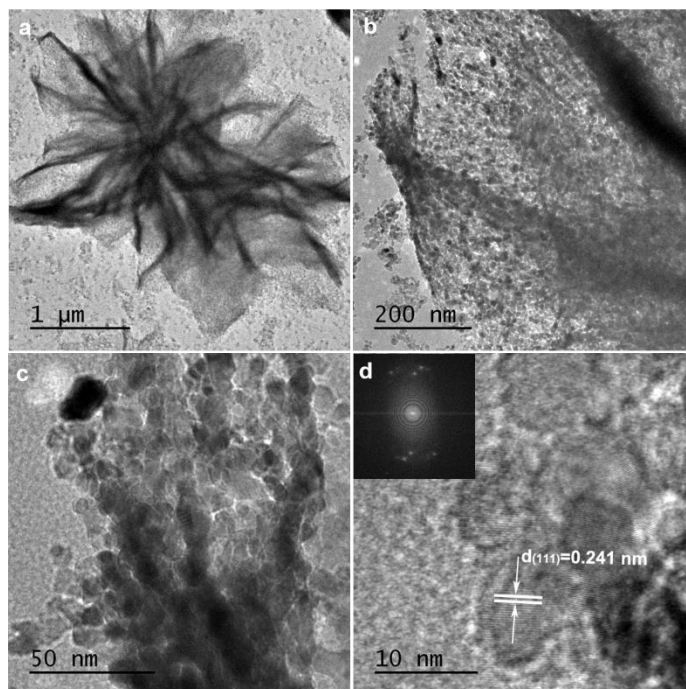


**Figure 4.** (a-c) TEM images of the NiO microflowers derived from Ni-PTA MOF, (d) HRTEM image of NiO microflowers.

The crystal structures of the as-synthesized samples were analyzed by the XRD technique and the XRD patterns were shown in Fig.5. The characteristic diffraction peaks present in the pattern at 37.25, 43.28, and 62.88°, can be indexed to the (111), (200), and (220) crystal face of NiO (JCPDS 47-1049). Compared with the XRD pattern of NiO nanorods obtained from Ni-BTEC, the wide diffraction peaks of NiO nanosheet-assembled microflowers indicated the little crystal size of NiO acquired from Ni-PTA MOF.

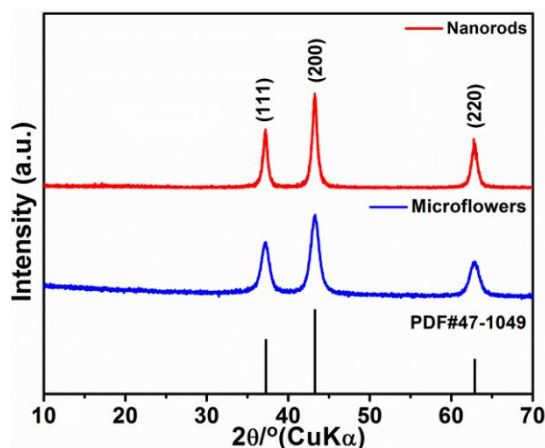


**Figure 5.** XRD patterns of NiO nanorods and microflowers.

The Brunauer-Emmet-Teller (BET) specific surface area of NiO nanorods and microflowers obtained from N<sub>2</sub> sorption isotherms, the typical hysteresis loop at the middle-pressure region was ascribed to the type IV isotherm, indicating the as-synthesized samples show a typical mesoporous structure. The BET surface area of NiO nanorods and microflowers is 38.25 and 123.49 m<sup>2</sup> g<sup>-1</sup>, respectively, with an average pore diameter of ~3.6 and 4.5 nm (inset in Fig.6a-b). The relatively high surface area and mesoporous architecture not only can provide efficient active sites but also promote the mass and electron transfer kinetics.

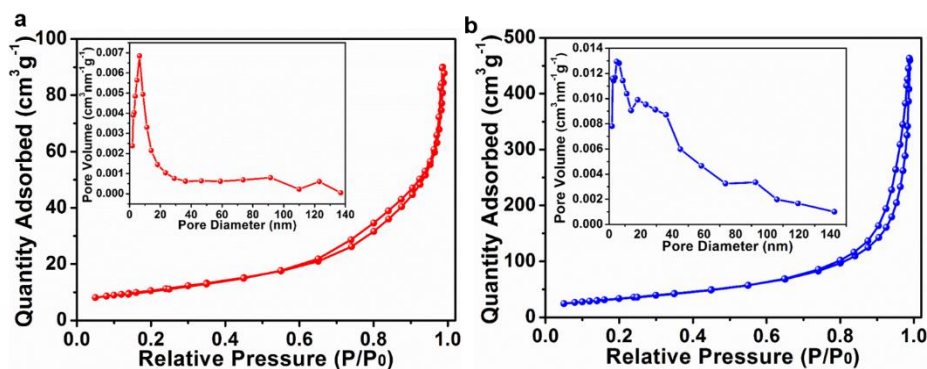
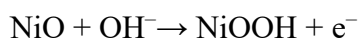


**Figure 6.** The N<sub>2</sub> sorption isotherms and pore size distribution of (a) NiO nanorods and (b) NiO microflowers.

### 3.1. Nonenzymatic-glucose sensor based on porous NiO nanorods and microflowers

The electrochemical performances of the porous NiO nanorods and microflowers were conducted in a typical three-electrode system in 0.1 M NaOH solution. At first, cyclic voltammogram (CV) measurements for NiO electrodes were conducted with the absence and presence of 0.1-2.0 mM glucose at a sweep of 50 mVs<sup>-1</sup> (Fig.7a-b). There is a distinct redox peak in each CV curve, which may attribute to the Faradaic oxidation/reduction reaction of Ni<sup>2+</sup> (NiO) and Ni<sup>3+</sup> (NiOOH) on the electrode surface. Upon injection of glucose, the porous NiO nanorods electrode demonstrates obvious a pair redox peak at ~0.36/0.53V, the oxidation currents of glucose show a steady increase with the boost glucose concentration and the anodic peak position upshift slightly. On the contrary, an obvious positive shift of the oxidation peak of NiO flowers with an increase in glucose concentration can be observed in Fig.7b, which indicated the decreases of glucose oxidation kinetics due to the oxidation of glucose molecules and some oxidized intermediates absorbed on the active sites, which cause the local pH change at the surface of NiO microflowers modified electrode [20, 21]. Thus, compared to NiO microflowers electrode, the porous NiO nanorods electrode may be an ideal glucose sensing materials. The anodic peak current of the two electrodes increases linearly with the addition of glucose, and the enhancement of anodic current may attribute to irreversible oxidation of glucose with the NiO catalysts. Simultaneously, the cathodic peak current of the two electrodes decrease due to the little consumption of Ni<sup>3+</sup> during the glucose electro-oxidation process [22]. The possible mechanism for glucose oxidation is illustrated as follows [23-26]:





In order to discover the relationship between the applied potential and the performance of the two sensors, the optimum operating potential was investigated in the presence of 0.1 mM glucose. The current response curves for different applied potentials shown in Fig.S1, 0.55 V was chosen as the applied potential for enzyme-free glucose determination, which is lower than NiO nanofibers obtained by electrospinning and calcination process [27], NiO coated carbon nanotubes (NiO/SCCNTs) synthesized by atomic layer deposition method [20], Ni-MOF/Ni/NiO/C nanocomposite obtained by one step calcination method [25].

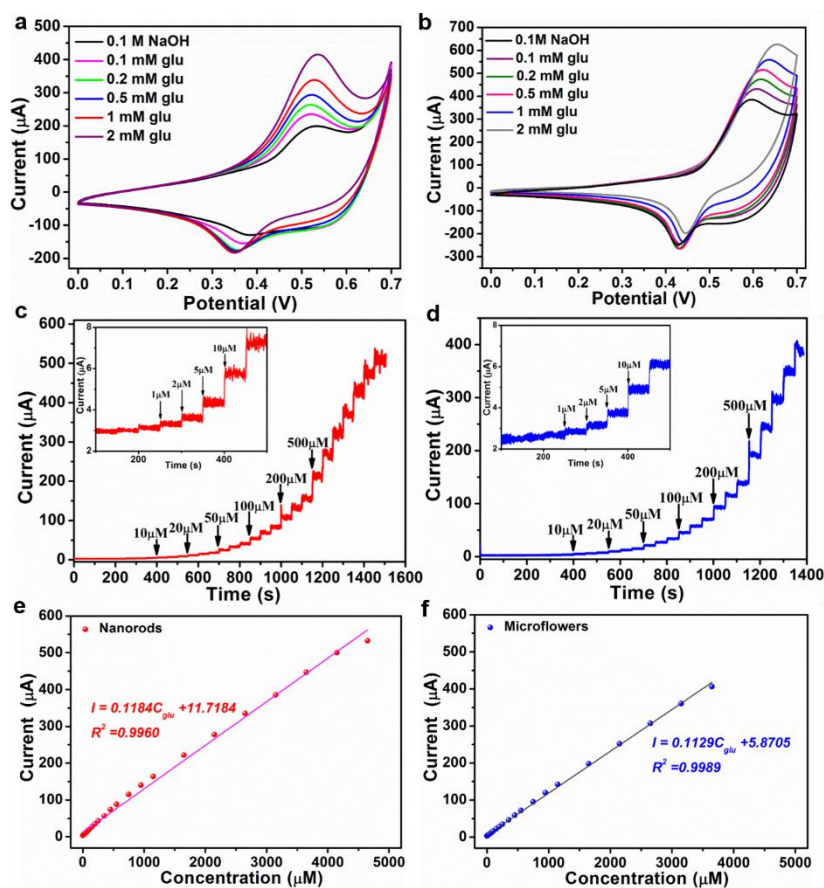


**Figure 7.** The cyclic voltammograms of NiO (a) nanorods and (b) microflowers in 0.1 M NaOH with different concentration of glucose. The chronoamperometry curves of NiO (c) nanorods and (d) microflowers at 0.55V vs. Ag/AgCl. The plots of response current density vs. glucose concentration (e) NiO nanorods and (f) NiO microflowers.

The glucose sensing performance of the two modified electrodes was evaluated via amperometric curve (i-t). Fig.7c-d show the representative amperometric response of NiO-GCE upon continuous injection of glucose into a stirring supporting electrolyte at a potential of 0.55 V. The response current increased sharply and rapidly to reach a stable platform when glucose was injected into the stirring electrolyte solution, suggesting a fast electron transfer rate between analyzer and NiO-GCE. As shown

in Fig. 7e, for the NiO nanorods electrode, the response current and glucose concentration can give a good linear relationship in a wide linear range of 0.0018 to 4.65 mM, which is superior to that of NiO microflowers electrode with the linear range of 0.0018 to 3.65 mM (Fig. 7f). The acquired linear equation of the former and the latter is  $I (\mu\text{A}) = 0.1184C (\mu\text{M}) + 11.7184$  ( $R^2=0.9960$ ) and  $I (\mu\text{A}) = 0.1129C (\mu\text{M}) + 5.8705$  ( $R^2=0.9989$ ), respectively. Furthermore, the low detection limit of NiO nanorods and microflowers electrode is calculated as 0.7 and 0.8  $\mu\text{M}$  ( $3\sigma/s$ ), respectively, and the corresponding sensitivity of the two NiO electrodes is 1.6775 and 1.5989  $\mu\text{A } \mu\text{M}^{-1} \text{ cm}^{-2}$ .

**Table 1.** The comparison of performances with other related sensors.

Electrode material	Potential (V)	Linear range/mM	Detection limit/ $\mu\text{M}$	Sensitivity/ $\mu\text{A } \text{mM}^{-1} \text{ cm}^{-2}$	Reference
NiO microflowers	0.55	0.0018-3.65	0.8	1598.9	This work
NiO nanorods	0.55	0.0018-4.65	0.7	1677.5	This work
NiCo <sub>2</sub> O <sub>4</sub> <sup>a</sup>	0.55	0.1-0.3 0.3-2.24	0.6	1917 703	18
NiO hollow Nanospheres <sup>b</sup>	0.35	1.5-7.0	47	343	19
NiO/SCCNTs <sup>c</sup>	0.65	0.002-2.2	0.1	1252.3	20
Ni(OH) <sub>2</sub> /3DGF <sup>d</sup>	0.55	0.001-1.7	0.34	2650	21
s-NiO/GD <sup>e</sup>	0.5	Up to 10	0.9	3613	22
NiO@PPy/Au	0.55	0.0005-1.7	0.15	802.9	23
Ni-MOF/Ni/NiO/C	0.65	0.84-5664	0.8	367.45	25
NiO/CC <sup>f</sup>	0.57	0.005-2.0	0.00745	4025	26
NiO nanofibers	0.6	0.002-0.60	0.77	1100	27
ZnO-NiO nanosheets/3D-KSCs <sup>g</sup>	0.5	0.013-4.86	4.12	448.6	28
Ni-Co NSs/RGO/GCE	0.5	0.01-2.65	6.83	878.05	29
NiO nanosheets	0.1 (vs. SMSE <sup>h</sup> )	0.0005-2.31	0.145	838.09	30
NiCo <sub>2</sub> O <sub>4</sub> nanorods	0.4	0.001-0.88	0.063	4710	31
Defect-rich Ni(OH) <sub>2</sub> /NiO nanosheet	0.6	0.09-1.08 1.08-3.62	5.0	2391.4 1371.9	32
NiCo <sub>2</sub> O <sub>4</sub> nanobelt/Ni Foam	0.45	0.0009-0.067 0.067-1.373	0.9	5000 727	33

(<sup>a</sup> 0.2 M NaOH, <sup>b</sup> immobilized glucose oxidase, <sup>c</sup> SCCNTs: stacked-cup carbon nanotubes, <sup>d</sup> 3DGF: three-dimensional graphene foam, <sup>e</sup> 0.5 M NaOH, <sup>f</sup> CC: carbon cloth, <sup>g</sup> KSCs: carbon derived from kenaf stem, <sup>h</sup> SMSE : saturated mercurous sulfate electrode)

Both the detection limit of sensors is lower than s-NiO/GD sensor (0.9  $\mu\text{M}$ ) [22], ZnO-NiO nanosheets/3D-KSCs sensor (4.12  $\mu\text{M}$ ) [28], and Ni-Co NSs/RGO/GCE sensor (6.83  $\mu\text{M}$ ) [29]. Moreover, the detection limit is at or below Ni-MOF/Ni/NiO/C sensor (0.8  $\mu\text{M}$ ) [25], and NiO nanosheets (0.145  $\mu\text{M}$ ) [30]. The sensitivity of the two NiO electrodes is higher than many NiO sensors

but inferior to that of NiCo<sub>2</sub>O<sub>4</sub> nanorods sensor (4710  $\mu\text{AmM}^{-1}\text{cm}^{-2}$ ) [31], defect-rich Ni(OH)<sub>2</sub>/NiO (2391.4  $\mu\text{AmM}^{-1}\text{cm}^{-2}$ ) [32], especially, the sensors constructed by conductive substrate, such as NiCo<sub>2</sub>O<sub>4</sub> nanobelt/Ni Foam sensor (5000  $\mu\text{AmM}^{-1}\text{cm}^{-2}$ ) [33], NiO/CC sensor (4025  $\mu\text{AmM}^{-1}\text{cm}^{-2}$ ) [26], Ni(OH)<sub>2</sub>/3DGF sensor (2650  $\mu\text{AmM}^{-1}\text{cm}^{-2}$ ) [21] in a relative low glucose concentration. The performance of glucose sensing for the two constructed NiO electrodes is comparable or better than the previously reported electrodes (Table1).

As a glucose electrochemical sensor, selectivity is an important parameter to assess if can be used for practical application, the chronoamperometric measurement (0.55V) was examined on the modified electrode against the common interference such as 20  $\mu\text{M}$  ascorbic acid (AA), uric acid (UA), dopamine (DA), NaCl, glutathione (GSH), and H<sub>2</sub>O<sub>2</sub>, the response current can be ignore compared with current response of 200  $\mu\text{M}$  glucose injected to 0.1 M NaOH supporting solution. The result showed that the

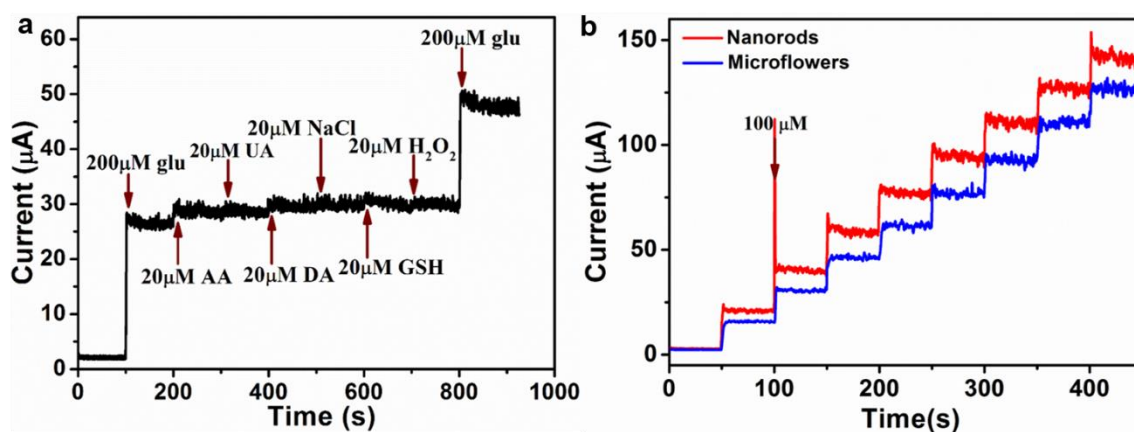


**Figure8.** (a) The anti-interference performance of the NiO nanorods electrode in detection of glucose. (b) The reproducibility of NiO nanorods and microflowers in 0.1 M NaOH with successive additions of 100  $\mu\text{M}$  glucose.

above interferences did not interfere with the determination of glucose with electrocatalytic oxidation reaction (Fig.8a and Fig.S2). Reproducibility and repeatability are crucial property of sensors for practical application. Thus, reproducibility and repeatability of the two NiO-GCE were also evaluated by chronoamperometric test via successive addition of 100  $\mu\text{M}$  standard glucose in 0.1M NaOH solution for eight time (Fig.8b). The acquired small value of RSD of NiO nanorods and microflowers are 4.14 and 5.07% respectively, indicating the sensors have good reproducibility and repeatability.

#### 4. CONCLUSIONS

In summary, nanoparticle-assembled hierarchical NiO nanorods and nanosheet-assembled microflowers have been successfully synthesized via a facile hydrothermal method and subsequent calcination. The NiO nanorods modified electrode revealed excellent electrocatalytic activity for glucose oxidation. The porous NiO nanorods modified electrode toward glucose nonenzymatic sensing exhibits several advantages include a wide linear detection range and good reproducibility. The research suggests that MOF-derived NiO porous nanorods may be used as an electrode material for glucose detection in the future.

## SUPPORTING INFORMATION

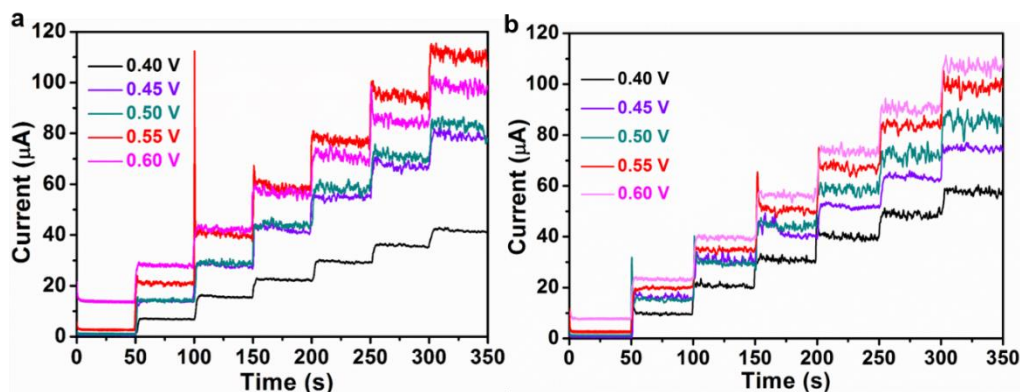


**Figure S1** The anodic current response of NiO electrodes at different applied potential, (a) NiO nanorods, and (b) NiO microflowers.

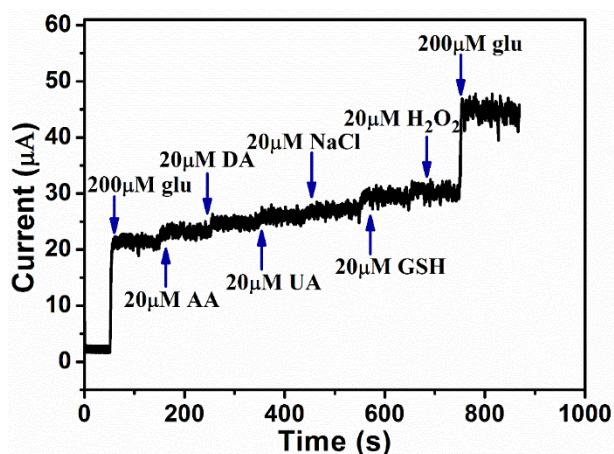


**Figure S2** The anti-interference of NiO microflowers electrode at 0.55 V.

## ACKNOWLEDGMENTS

This work was financially supported by the National Science Foundation of China (No. 21603004, U1604119), the Program for Innovative Research Team of Science and Technology in the University of Henan Province (18IRTSTHN006), and the Natural Science Foundation of Henan Province (182300410194).

## References

1. G. F. Wang, X. P. He, L. L. Wang, A. X. Gu, Y. Huang, B. Fang, B. Y. Geng, X. J. Zhang, *Microchim. Acta*, 180 (2013)161–186.
2. P. Si, Y. J. Huang, T. H. Wang, J. M. Ma, *RSC Adv.*, 3 (2013) 3487–3502.
3. K. Dhara, D. R. Mahapatra, *Microchim. Acta*, 185 (2018) 49.
4. S. Liu, B. Yu, T. Zhang, *Electrochim. Acta*, 102 (2013)104–107.

5. N. Singer, R. G. Pillai, A. I. D. Johnson, K. D. Harris, A. B. Jemere, *Microchim. Acta*, 187 (2020)196.
6. J. Song, L. Xu, C. Y. Zhou, R. Q. Xing, Q. L. Dai, D. L. Liu, H. W. Song, *ACS Appl. Mater. Interfaces*, 5 (2013) 12928–12934.
7. X. D. Liu, Y. Yang, R. Y. Liu, Z. L. Shi, L. Y. Ma, M. Wei, *J. Alloys Compd.*, 718 (2017) 304–310.
8. M. Kang, H. Zhou, N. Zhao, B. L. Lv, *CrystEngComm*, 22 (2020) 35–43.
9. H. Y. Xu, C. K. Xia, S. Y. Wang, F. Han, M. Karbalaee Akbari, Z. Y. Hai, S. Zhuiykov, *Sensors and Actuators B*, 267 (2018) 93–103.
10. D. Cheng, T. Wang, G. X. Zhang, H. M. Wu, H. Mei, *J. Alloys Compd.*, 819 (2020) 153014.
11. M. Saraf, K. Natarajan, S. M. Mobin, *New J. Chem.*, 41 (2017) 9299–9313.
12. J. Zhang, Y. D. Sun, X. C. Li, J. S. Xu, *J. Alloys Compd.*, 831 (2020) 154796.
13. A. Heller, B. Feldman, *Chem. Rev.*, 108 (2008) 2482–2505.
14. B. L. Ellis, P. Knauth, T. Djenizian, *Adv. Mater.*, 26 (2014) 3368–3397.
15. Y. Liu, X. C. Li, W. M. Shen, Y. Dai, W. Kou, W. J. Zheng, X. B. Jiang, G. H. He, *Small*, 15 (2019) 1804737.
16. Y. Shu, Y. Yan, J. Y. Chen, Q. Xu, H. Pang, X. Y. Hu, *ACS Appl. Mater. Interfaces*, 9 (2017) 22342–22349.
17. Y. M. Luo, Q. Y. Wang, J. H. Li, F. Xu, L. X. Sun, Y. T. Bu, Y. J. Zou, H.-B. Kraatz, F. Rosei, *Inorg. Chem. Front.*, 7 (2020) 1512–1525.
18. W. Huang, Y. Cao, Y. Chen, J. Peng, X. Y. Lai, J. C. Tu, *Appl. Surf. Sci.*, 396 (2017) 804–811.
19. C. C. Li, Y. L. Liu, L. M. Li, Z. F. Du, S. J. Xu, M. Zhang, X. M. Yin, T. H. Wang, *Talanta*, 77 (2008) 455–459.
20. M. H. Raza, K. Movlaee, Y. L. Wu, S. M. El-Refaei, M. Karg, S. G. Leonardi, G. Neri, N. Pinna, *ChemElectroChem*, 6 (2019) 383–392.
21. B. B. Zhan, C. B. Liu, H.P. Chen, H. X. Shi, L. H. Wang, P. Chen, W. Huang, X. C. Dong, *Nanoscale*, 6 (2014) 7424–7429.
22. H. Liu, X. L. Wu, B. Yang, Z. J. Li, L.C. Lei, X. W. Zhang, *Electrochimi. Acta*, 174 (2015) 745–752.
23. J. Chen, Q. L. Sheng, J. B. Zheng, *RSC Adv.*, 5 (2015) 105372–105378.
24. D. Saravana achari, C. Santhosh, R. Deivasegamani, R. Nivetha, A. Bhatnagar, S. K. Jeong, A. N. Grace, *Microchim. Acta*, 184 (2017) 3223–3229.
25. Y. Shu, Y. Yan, J. Y. Chen, Q. Xu, H. Pang, X. Y. Hu, *ACS Appl. Mater. Interfaces*, 9 (2017) 22342–22349.
26. F. L. Zhou, Q. Wang, K. Huang, X. Jiang, Z. R. Zou, X. L. Xiong, *Microchem. J.* 159 (2020) 105505.
27. Y. Q. Zhang, Y. Z. Wang, J. B. Jia and J. G. Wang, *Sensors and Actuators B*, 171–172 (2012) 580–587.
28. Y. Y. Zhang, L. Wang, J. Yu, H. Yang, G. X. Pan, L. F. Miao, Y. H. Song, *J. Alloys Compd.*, 698 (2017) 800–806.
29. L. Wang, X. P. Lu, Y. J. Ye, L. L. Sun, Y. H. Song, *Electrochimi. Acta*, 114 (2013) 484–493.
30. M. M. Guo, L. B. Wei, Y. H. Qu, F. Y. Zeng, C. L. Yuan, *Mater. Lett.*, 213 (2018) 174–177.
31. M. Saraf, K. Natarajana, S. M. Mobin, *New J. Chem.*, 41 (2017) 9299–9313.
32. W. Huang, L.Y. Ge, Y. Chen, X.Y. Lai, J. Peng, J. C. Tu, Y. Cao, X. T. Li, *Sensors and Actuators B*, 248 (2017) 169–177.
33. J. Zhang, Y. D. Sun, X. C. Li, J. S. Xu, *J. Alloys Compd.*, 831 (2020) 154796.